Theoretical calculations of K-edge absorption spectra in warm dense Al

2008 J. Phys.: Condens. Matter 20 195211

(http://iopscience.iop.org/0953-8984/20/19/195211)

IOP PUBLISHING JOURNAL OF PHYSICS: CONDENSED MATTER

J. Phys.: Condens. Matter **20** (2008) 195211 (9pp) doi:10.1088/0953-8984/20/19/195211

Theoretical calculations of K-edge absorption spectra in warm dense Al

O Peyrusse

CELIA, Université Bordeaux I, CNRS, CEA, 351 Cours de la Libération, 33405 Talence, France

E-mail: peyrusse@celia.u-bordeaux1.fr

Received 21 December 2007, in final form 18 March 2008
Published 11 April 2008
Online at stacks.iop.org/JPhysCM/20/195211

Abstract

Theoretical calculations of the shape of an absorption edge in a warm dense simple material such Al are described. The calculations include the XAFS (x-ray absorption fine structure) features above the edge. The shape of these modulations relates to the atomic spatial distribution and to the electronic density of states (DOS) in the continuum. The underlying warm dense plasma model is based on a density-functional neutral pseudoatom approach which gives the radial distribution function (RDF) and the electron density around one specific site. Combined with a full multiple-scattering (MS) approach giving the final free wavefunction in a photoionization process, the model is used to predict the shape of photoabsorption K edges over a range of compression ratios from 0.5 to 3 and temperatures from 0.1 to 10 eV. It is found that XAFS structures are intense enough to be observable for densities of the order of (and above) the solid density and that dynamic or static absorption spectroscopy measurements could provide interesting information on the warm dense matter regime.

1. Introduction

The physical properties of warm dense matter are still poorly known in comparison with the solid state and with the hot plasma state. The reason is both experimental and theoretical. The very transient state of this regime makes laboratory experiments very difficult and the subsequent lack of reliable experimental data does not give firm foundations to the theoretical models of this state of matter, which is characterized by strong correlations. Experimental studies on the equation of state, reflectivity, electrical conductivity and x-ray scattering [1–6] already give interesting data points to be compared with theory [7–10]. However, there is a need for measurements that involve more directly the structural properties of this strongly coupled regime.

In this paper, we explore the possibility of using the structure of a photoabsorption edge to get information on the electronic and structural properties such as the pair correlation function. Previous experimental measurements [11, 12] or theoretical calculations [13] of the K edge in dense compressed material have already been reported. A recent study of the K edge in dense but significantly heated Al must also be quoted [14]. These studies focused mainly on the position and the width of the edge, i.e. in an energy zone close to the onset of absorption. Here, by calculating the whole absorption edge, which includes specific features well known in solid-state physics such as the so-called *x-ray absorption near-edge spectroscopy* (XANES) structures above the edge, we show how very careful measurements of this threshold could provide other data points for a better understanding of warm dense matter. To our knowledge, this is the first systematic study of XANES spectra in the warm dense regime.

Present calculations are based on a multiple-scattering approach to the photoionization process, combined with a density-functional-theory (DFT) approach to the dense plasma state. This last method has already proven to be very fruitful for calculating various physical properties of dense plasmas and of liquid metals. Such an approach considers the *correlation sphere* around a central ion as the physically relevant volume (instead of the ion-sphere or Wigner–Seitz volume). In the calculations, this correlation sphere radius is only large enough to insure that the ion distribution function is unity on the edge of the calculation sphere. Starting from the temperature T and from the density ρ, the DFT approach consists mainly in solving self-consistently two sets of equations. The first set models the electron density distribution in the potential of the central ion by solving effective one-particle Schrödinger equations. The second set of equations used for the ion

distribution has the form of the hypernetted-chain (HNC) equations with an effective ion–ion pair interaction built within the neutral pseudoatom (NPA) model. The first set of equations provides the atomic structure of the *average atom* in the plasma as well as various electronic quantities. The second one gives the ion–ion radial distribution function $g(r)$. Such an approach, where the full finite-temperature response of the ions and of the electrons is treated in a self-consistent manner, goes well beyond the one-component-plasma (OCP) approach, where the electrons are merely a static neutralizing background. A general conclusion of the calculations is that authorizing the electrons to respond gives to the whole system the behavior of a lower density OCP. It is worth noting that such an approach is clearly distinct from the heavy quantum molecular dynamics (QMD) simulations [15–19], where the electrons are treated by the Kohn–Sham theory while a convenient number of ions are made to evolve in time.

From this model of dense matter, the subsequent step of the calculations consists in evaluating the photoionization cross section of a bound electron (here on K-shell) for a significative number of energy points around the edge. This step involves a careful determination of the final free wavefunction. This has been achieved in a full multiple-scattering (MS) approach from selected sets of ion configurations that sample the previously obtained radial distribution function.

Section 2 presents the theoretical background of full multiple-scattering calculations. In section 3, we outline the finite-temperature DFT approach to dense matter with an application to structural properties of warm dense aluminum. Then, special attention is paid to the questions of potential construction and threshold position that arise in multiple-scattering photoionization calculations. In section 4, theoretical calculations of K-edge spectra will be given and discussed. Section 5 is a conclusion of this work.

2. Full multiple-scattering K-edge photoionization cross section

The starting point of our calculations is a convenient description of the photoionization process occurring in a dense material. In this work, we calculate the photoionization cross section in the framework of the multiple-scattering theory (MST) in a muffin-tin (MT) potential. In its usual form, the MST is used to compute the final wavefunction of the photoelectron in the ionization process. A crucial aspect here lies in the necessary 'muffin-tinization' of the potential experienced by the photoelectron. The construction of this potential from 'real' configurations of neighboring atoms as well as the limitations introduced by the MT approximation are discussed later in the text (section 3.4). The photoabsorption is governed by the dipole matrix element between a strongly localized initial state i (the core electron) and a final state f describing the delocalized photoelectron. More precisely, the general expression for the *configuration averaged* photoabsorption cross section of an electron being in the subshell ℓ_i (of occupation n_i) reads

$$\sigma_{\rm o}(E) = \frac{n_i}{4\ell_i + 2} \sum_{m_i} \sum_{\ell_f, m_f} \sigma_{if}(E) \tag{1}$$

where i, f refers two Slater determinants that differ in one orbital, a bound orbital $\psi_{\ell_i m_i}$ in state i and a free wavefunction $\psi_{\ell_f m_f, k}$ in state f with wavenumber k. Then, one has

$$\sigma_{if}(E) = a\,E \sum_{q=0,\pm1} |\langle \psi_{\ell_i m_i} | r_q^{(1)} | \psi_{\ell_f m_f, k} \rangle|^2 \left(1 - f_{\rm F}\left(\frac{X}{kT}\right)\right) \tag{2}$$

with $r_q^{(1)} = \sqrt{\frac{4\pi}{3}}\, r\, Y_{1q}(\hat{r})$ (Y_{1q} is a usual spherical harmonic). One defines $\epsilon = E - E_{\rm o}$ as the kinetic energy of the photoelectron, $E_{\rm o}$ being the onset of absorption. If the photon energy E is in Rydberg, the cross section in cm^2 and the free wavefunction normalized such that the asymptotic amplitude is $\epsilon^{1/4}$ ($k = \sqrt{\epsilon}$), the numerical coefficient a has the value $a = 8.56 \times 10^{-19}$. $f_{\rm F}$ is the Fermi occupation factor depending on X so that $1 - f_{\rm F}(X/kT)$ is the vacancy available for the photoelectron. If ϵ (> 0) is the energy of the photoelectron relative to the (constant) value of the muffin-tin interstitial potential (*that we define as the onset of absorption*), X is the energy of the photoelectron relative to the chemical potential μ. Note that for K-shell photoabsorption one has $n_i = 2$, $\ell_i = m_i = 0$, hence $\ell_f = 1$, $m_f = 0, \pm 1$.

The final state $\psi_{\ell_f m_f, k}$ depends on the nature and the position of the atoms neighboring the absorbing atom and we have to deal with the difficulty of calculating a photoelectron wavefunction by representing the potential as a cluster of spherical potentials centered on the atomic sites. Here, we used the multiple-scattering theory (MST) to treat the interaction of the photoelectron with the set of neighboring scatterers. Essentials of this theory can be found elsewhere [20, 21]. In this work, we used a form of the MST that is also called the scattered wave method in real space. A very clear presentation of this approach can be found in [22]. Another form of the theory, the Green function method, also exists, and the interested reader will find practical details in [23, 24]. In the scattered wave method, the final state wavefunction is computed as being the sum of two parts: an outgoing wave plus a sum of scattered waves. We consider a real finite cluster of N atoms (*real* means here that one considers a specific spatial configuration of atoms). The absorbing atom is supposed to be at the center of the cluster. *Inside* each atomic sphere the potential is purely radial and the Schrödinger equation can be solved numerically for each wave (ℓ', m') so that the free wavefunction reads

$$\psi_{\ell_f m_f, k}(\mathbf{r}) = \sum_{\ell' m'} B_{\ell' m'}(\ell_f m_f) R_{\ell', k}(r) Y_{\ell' m'}(\hat{r}) \tag{3}$$

where $R_{\ell', k}(r)$ is the numerical solution of the radial Schrödinger equation for the wavenumber k, $Y_{\ell' m'}(\hat{r})$ is a spherical harmonic and the $B_{\ell' m'}(\ell_f m_f)$ are a set of coefficients necessary to ensure the continuity of $\psi_{\ell_f m_f, k}(\mathbf{r})$ and its first derivative at the frontier of the atomic sphere. In the *interstitial* region, the potential is supposed to be constant (within the muffin-tin approximation, see below) and we consider that each function $\psi_{\ell_f m_f, k}(\mathbf{r})$ can be expressed as

$$\psi_{\ell_f m_f, k}(\mathbf{r}) = j_{\ell_f}(kr) Y_{\ell_f m_f}(\hat{r}) - \mathrm{i} \sum_j \sum_{\ell' m'} B^{(j)}_{\ell' m'}(\ell_f m_f) h^+_{\ell'}(r_j) Y_{\ell' m'}(\hat{r}_j) \tag{4}$$

where j_ℓ is a spherical Bessel function and the $h^+_{\ell'}(r_j)$ are Hankel functions centered on atomic site j. In this equation j runs over the number of atoms in the cluster while ℓ' runs in principle from zero to infinity. Coefficients $B^{(j)}_{\ell' m'}(\ell_f m_f)$ are determined by imposing continuity conditions for the wave $\psi_{\ell_f m_f, k}(\mathbf{r})$ and its first derivative at the border of the atomic spheres. In practice, the summations are truncated to a given $\ell_{\max}$, whose value is determined by the rule $\ell_{\max} \approx r_{\mathrm{MT}} k$, r_{MT} being the radius of the atomic spheres in the muffin-tin potential. In our calculation, we found that $\ell_{\max} = 5$ was sufficient for having converged results for photoelectrons of a few tens of eV. Imposing the continuity conditions leads to a $N(\ell_{\max}+1)^2 \times N(\ell_{\max}+1)^2$ complex linear system for the $B^{(j)}_{\ell' m'}(\ell m)$ [22]. Of course, such a system must be built and solved for each value of wavenumber k.

Until now, the calculations ignore both the finite core–hole duration as well as the finite mean free path of the photoelectron in the material. Both effects are taken into account by convolving σ_{o} by a Lorentzian and writing for the actual cross section

$$\sigma(E) = \frac{1}{2\pi} \int_{-\infty}^{+\infty} \frac{\Gamma(E')}{(E-E')^2 + \Gamma(E')^2/4} \sigma_{\mathrm{o}}(E')\, \mathrm{d}E' \quad (5)$$

where $\Gamma(E) = \Gamma_{\mathrm{hole}} + \Gamma_{\mathrm{el}}(E)$. For K-shell ionized aluminum, the Auger width is $\Gamma_{\mathrm{hole}} = 0.6$ eV [25]. The second contribution $\Gamma_{\mathrm{el}}(E) = \frac{\hbar}{\lambda_{\mathrm{el}}(\epsilon)}\sqrt{2\epsilon/m}$ is related to the photoelectron mean free path $\lambda_{\mathrm{el}}(\epsilon)$. $\epsilon = E - E_{\mathrm{o}}$ is the kinetic energy of the photoelectron (E_{o} being the onset of absorption). Starting from the electron self-energy in an electron gas, careful estimations of $\lambda_{\mathrm{el}}(\epsilon)$ have been published by Penn [26]. It is important to note here that the time dependence of the formation and relaxation of the absorption edge profile is not considered in these calculations. Approaches for evaluating the importance of these time-dependent effects can be mentioned [27, 28]. However, K-edge absorption spectra in dense materials do not seem very sensitive to these effects.

In the next section, we present the *structural aspects* underlying our calculations of the photoionization cross section, namely, the distribution of the neighboring atoms around the photoionized atom and the construction of the potential seen by the photoelectron.

3. Description of warm dense matter using the Kohn–Sham equations

The DFT approach presented here is very close to the implementation point of view and thus rather phenomenological. For a more rigorous presentation of the DFT equations in dense plasmas, the interested reader will refer to [29]. The approach makes use of the neutral pseudoatom (NPA) concept which provides a natural separation between the ions and the electrons. We will see how it takes place in standard calculations of XANES spectra.

3.1. NPA pair interaction and structural property calculations

The neutral pseudoatom method consists in assuming that the total electron density $\rho_{\mathrm{cluster}}(\mathbf{r})$ of an actual cluster of atoms (ultimately a metal or a liquid metal) can be written as a sum of localized electron densities that follow the ions in their movement

$$\rho_{\mathrm{cluster}}(\mathbf{r}) = \sum_i \rho^{(1)}_{\mathrm{el}}(|\mathbf{r} - \mathbf{R}_i|) \quad (6)$$

where $\mathbf{R}_i$ is the position of the ion site i and $\rho^{(1)}_{\mathrm{el}}$ is the 'one site' electron density. This superposition approximation (common in condensed-matter physics) is consistent with the binary character of the interatomic forces. Furthermore, one separates *core* electrons from *valence* electrons, i.e.,

$$\rho^{(1)}_{\mathrm{el}}(\mathbf{r}) = \rho_{\mathrm{c}}(\mathbf{r}) + \Delta\rho(\mathbf{r}) \quad (7)$$

where $\Delta\rho(r)$ is the valence charge *per atom*. One has $\int \Delta\rho(r)\, \mathrm{d}\mathbf{r} = Z^*$ and $\int \rho^{(1)}_{\mathrm{el}}(\mathbf{r}), \mathrm{d}\mathbf{r} = Z$. Z^* is the effective charge of the ions. Of course, these 'atoms' or 'neutral pseudoatoms' are not the same as the objects we get if we take the cluster to pieces and put the right number of valence electrons around each ion [30]. This is because the electrons of the electron gas (in which the ions are immersed) tend to distribute so as to form screening clouds about each ion. The 'one atom' quantities $\rho_{\mathrm{c}}(\mathbf{r})$ and $\Delta\rho(\mathbf{r})$ are usually obtained from a specific DFT–Kohn–Sham calculation through a *pseudopotential* w (section 3.2). For liquid metals, discarding the 'core' electrons, a model *pseudopotential* can also be used to obtain $\Delta\rho(r)$ [31]. Whatever the method we use, one can show, from a second order calculation of the total energy of the system (ions + electrons), that the pair potential reads $\phi_{\mathrm{eff}}(\mathbf{r}) = \frac{Z^{*2}}{r} + \phi_{ps}(\mathbf{r})$, where $\phi_{ps}(\mathbf{r})$ is the Fourier transform of the product $\Delta\tilde{\rho}(\mathbf{q})\tilde{w}(\mathbf{q})$. Finally, the pair potential reads

$$\phi_{\mathrm{eff}}(\mathbf{r}) = \frac{Z^{*2}}{r} + \frac{1}{(2\pi)^3} \int \mathrm{e}^{-\mathrm{i}\mathbf{q}\cdot\mathbf{r}} \Delta\tilde{\rho}(\mathbf{q})\tilde{w}(\mathbf{q})\, \mathrm{d}\mathbf{q}. \quad (8)$$

From this pair interaction, and assuming that the ions behave classically, one may invoke the classical theory of liquids where the radial distribution function $g(r)$ is obtained from the following set of equations:

$$h(r) = g(r) - 1 = n_i \int \mathrm{d}\mathbf{r}' c(r') h(r - r') + c(r) \quad (9)$$

$$g(r) = \exp\left[-\frac{\phi_{\mathrm{eff}}}{kT} + h(r) - c(r) + B(r) \right]. \quad (10)$$

Equation (9) is the Ornstein–Zernicke equation while equation (10) is the so-called hypernetted-chain (HNC) closure relation. $c(r)$ is the direct correlation function and n_i is the ion density. The strict HNC scheme corresponds to $B(r) = 0$ where $B(r)$ is the so-called *Bridge function* (the sum of elementary graphs). If $B(r) \neq 0$ one speaks of *modified* HNC (MHNC). Thus, the HNC treatment can be improved by choosing a convenient bridge function [32], and this is crucial for strongly correlated systems. A well known method for calculating $B(r)$ is based on the observation of the following universality principle [32]: 'The Bridge functions constitute the same family of curves, irrespective of the assumed pair potential'. Following this universality principle, one can invoke a *reference system* having a well defined pair

interaction and for which a parametrized radial distribution $g(r)$ is available (from many MD or MC simulations). The best known system is the so-called hard-sphere (HS) system, whose pair interaction is simply given by $\phi_{\rm eff}(r) = \infty$ for $r < \sigma$; $\phi_{\rm eff}(r) = 0$ for $r > \sigma$. Verlet and Weiss [33] have given a good fit of the radial distribution $g_{\rm HS}(r, \eta)$ as a function of the *packing fraction* $\eta = \frac{1}{6}\pi n_i \sigma^3$. An independent fit of the hard-sphere bridge function $B_{\rm HS}(r, \eta)$ is also available [34]. Having chosen the hard-sphere reference system, the best choice of the packing fraction η remains. The best *a priori* choice has been proposed by Lado *et al* [35], showing that a minimization of the (modified) HNC free energy of a system of particles interacting through a given pair potential $\phi_{\rm eff}$ leads to the following condition for η:

$$\int {\rm d}\mathbf{r}[g(r) - g_{\rm HS}(r, \eta)]\frac{{\rm d}B_{\rm HS}(r, \eta)}{{\rm d}\eta} = 0. \tag{11}$$

Equation (11) must be added to the set of equations (9) and (10).

3.2. NPA pseudopotential

We give here some details about the method used for obtaining the pseudopotential $\tilde{w}(q)$ and the valence charge (per atom) which are involved in the pair interaction determination (equation (8)). As mentioned above, a possible method makes use of a model pseudopotential. The linear response of an electron gas to a weak pseudopotential reads

$$\Delta\tilde{\rho}(q) = \frac{\pi_{\rm o}(q)}{\epsilon(q)}\tilde{w}(q) \tag{12}$$

in which $\pi_{\rm o}(q) = -\frac{k_{\rm F}}{\pi^2}(\frac{1}{2} + \frac{1-b^2}{4b}\log|\frac{1+b}{1-b}|)$ is the RPA polarizability ($b = q/2k_{\rm F}$), $\epsilon(q) = 1 - \frac{4\pi}{q^2}[1 - G(q)]\pi_{\rm o}(q)$ is the static dielectric function and $k_{\rm F}$ is the Fermi wavevector. $G(q)$ is the local-field correction, allowing us to take into account exchange–correlation effects (for a recent discussion see [36]). A quite simple expression for this local-field correction has been given by Taylor [37]: $G(q) = \frac{q^2}{4k_{\rm F}^2}[1 + \frac{0.1534}{\pi k_{\rm F}}]$. $\Delta\tilde{\rho}(q)$ being obtained from $\tilde{w}(q)$ (equation (12)), one easily gets $\phi_{\rm eff}$ from equation (8).

In order to get rid of any 'ad hoc' model pseudopotential, we used in the present work the model of the *ion in a jellium vacancy* [29, 38] that gives $\Delta\tilde{\rho}(q)$, an effective pseudopotential and finally the pair interaction. The SCF valence charge *per atom* $\Delta\rho^{\rm SCF}$ is obtained by writing the 'one site' electron density as the difference (right term)

$$\rho_{\rm el}^{(1)}(\mathbf{r}) = \rho_{\rm c}(\mathbf{r}) + \Delta\rho^{\rm SCF}(\mathbf{r}) = \rho_{\rm el}(\mathbf{r}) - \rho_v(\mathbf{r}) \tag{13}$$

where the electronic density $\rho_{\rm el}(\mathbf{r})$ has the (average-atom) form

$$\rho_{\rm el}(r) = \sum_{\rm b} f_{\rm F}(\epsilon_{\rm b})|\phi_{\rm b}|^2 + \sum_{\ell}\int_{\rm o}^{\infty} f_{\rm F}(\epsilon_\ell)|\phi_{\ell,\epsilon}|^2\,{\rm d}\epsilon \tag{14}$$

in which the first sum runs over the bound orbitals ($\epsilon_{\rm b} < 0$) while the second runs over the free orbitals ($\epsilon > V(R_{\rm c})$). Function $f_{\rm F}$ is the usual Fermi occupation factor $f_{\rm F}(\epsilon) = (1 + {\rm e}^{(\epsilon-\mu)/kT})^{-1}$. One-electron orbitals ϕ are obtained by solving the radial Schrödinger equation with the potential V

$$V(\mathbf{r}) = \int_{\rm o}^{R_c}\frac{\rho_{\rm el}(\mathbf{r}') - n_+(\mathbf{r}')}{|\mathbf{r} - \mathbf{r}'|}\,{\rm d}\mathbf{r}' + V_{\rm xc}[\rho_{\rm el}] \tag{15}$$

where

$$n_+(\mathbf{r}) = Z\delta(\mathbf{r}) + Z^* n_i \Theta(\mathbf{r} - \mathbf{r}_{\rm ws}) \tag{16}$$

is the density of positive charge. $R_{\rm c}$ is here a correlation sphere radius of the order of a few $r_{\rm ws}$ (the ion-sphere radius). An independent calculation with the positive density of charge (the spherical cavity alone)

$$n_+(\mathbf{r}) = Z^* n_i \Theta(\mathbf{r} - \mathbf{r}_{\rm ws}), \tag{17}$$

gives $\rho_v(\mathbf{r})$. In equation (13) $\rho_{\rm c}(\mathbf{r}) = \sum_{\rm b} f_{\rm F}(\epsilon_{\rm b})|\phi_{\rm b}(\mathbf{r})|^2$, while in equations (16) and (17) Θ is the Heaviside function. One considers now the pseudopotential w^* giving $\Delta\rho^{\rm SCF}$ in the linear response, i.e. $\Delta\tilde{\rho}^{\rm SCF}(q) = \frac{\pi_{\rm o}(q)}{\epsilon(q)}\tilde{w}^*(q)$. In practical calculations, the oscillations of $\Delta\rho^{\rm SCF}(\mathbf{r})$ into the core region lead to too large components (for large q) of the Fourier transform. Before performing the Fourier transform of $\Delta\rho^{\rm SCF}(\mathbf{r})$, a preliminary smoothing inside the core is necessary. Such a smoothing is achieved by taking $\Delta\rho(\mathbf{r}) = A - Br^2$ for $r \leqslant r_{\rm c}$, otherwise $\Delta\rho(\mathbf{r}) = \Delta\rho^{\rm SCF}(\mathbf{r})$. A, B are chosen so that $\Delta\rho(\mathbf{r})$ and its derivative are continuous at $r = r_{\rm c}$. Then, $\Delta\rho(\mathbf{r})$ must be normalized so that $\int \Delta\rho(r)\,{\rm d}\mathbf{r} = Z^*$ is satisfied. Note that the results are not sensitive to the choice of $r_{\rm c}$ as long as one takes $r_{\rm c}$ of the order of unity (in au) for Al.

It is worth noting that the average-atom description of the electron density comes from a finite-temperature DFT description of the problem. For the determination of Z^*, the most reasonable choice consists in defining a neutrality radius R_n such as $\int_{\rm o}^{R_n}\rho_{\rm el}\,{\rm d}\mathbf{r} = Z$. Effective charge Z^* is thus simply given by $Z^* = Z - \int_{\rm o}^{R_n}\rho_{\rm bound}(r)\,{\rm d}\mathbf{r}$, where $\rho_{\rm bound}$ is just the first sum of the right part of equation (14). Also, the chemical potential μ is determined from the requirement of the neutrality of the correlation sphere

$$\int_{\rm o}^{R_c}\rho_{\rm el}(\mathbf{r})\,{\rm d}\mathbf{r} = 0. \tag{18}$$

Last, the simple Kohn–Sham functional $V_{\rm xc}[\rho_{\rm el}] = (\frac{3}{\pi}\rho_{\rm el})^{1/3}$ has been used throughout this work.

3.3. Structural results in warm dense Al

We applied the above principles to Al, for which proper absorption experiments can be hoped for. More precisely, we applied the above DFT model with an NPA pair interaction (section 3.1) and the self-consistent determination of the valence charge per atom $\Delta\rho^{\rm SCF}(r)$ that gives the effective pseudopotential w (section 3.2). The quantities we extract from the above dense matter model are the needed atomic orbitals, i.e. the 1s orbital for K-shell calculations, the NPA bound and valence densities (see equation (7)) and the radial distribution function (RDF). We will see in the next part (section 3.4) how these basic ingredients are used to build

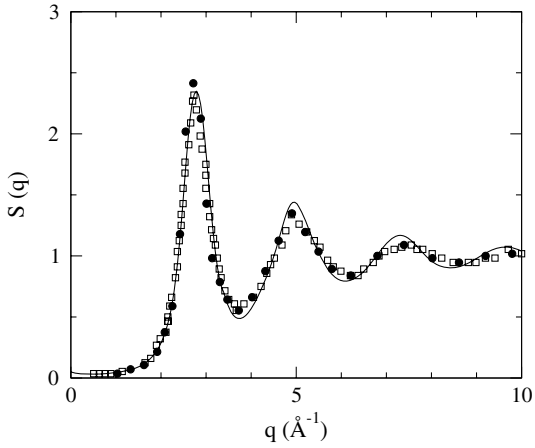

Figure 1. The static structure factor of liquid Al ($\rho = 2.37$ g cm^{-3}, $T = 0.086$ eV). Solid dots: x-ray diffraction data [35]. Squares: QMD simulations [17]. Continuous line: present calculations.

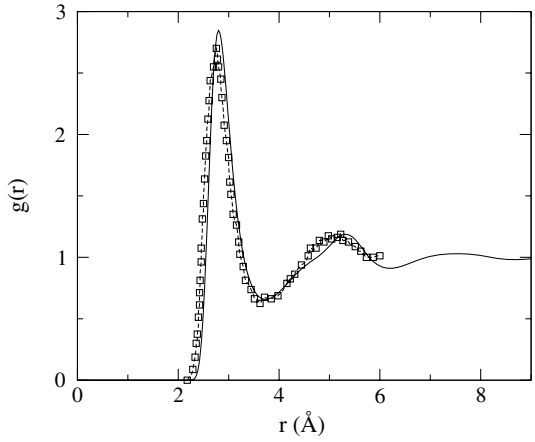

Figure 2. Radial distribution function of Al at ($\rho = 2.0$ g cm^{-3}, $T = 0.086$ eV). Squares: QMD simulations [16]. Continuous line: present calculations.

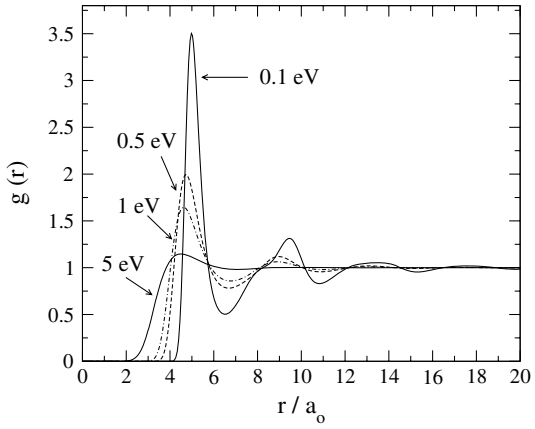

Figure 3. The temperature dependence of the ion–ion RDF of Al at solid density (ρ_o) for a range from 0.1 to 5 eV. For all of these cases, $Z^* = 3$. a_0 is the Bohr radius.

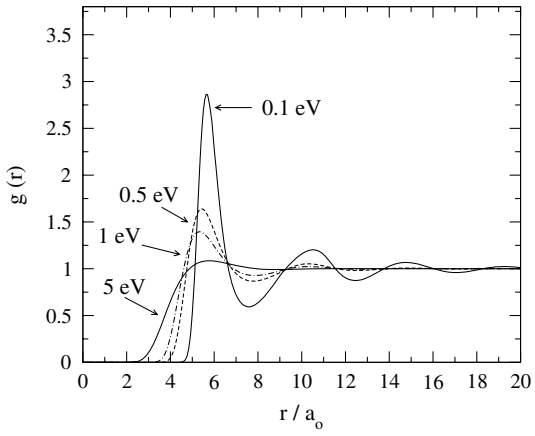

Figure 4. The temperature dependence of the ion–ion RDF of Al at $\rho_o/2$ for a range from 0.1 to 5 eV. For all of these cases, $Z^* = 3$.

a photoionization profile. All the cases presented in this study correspond to a density–temperature range where the ionization Z^* is non-ambiguous and equal to three. The previous DFT model predicts such an established fact for temperatures between 0.1 and 10 eV and compressions between 0.5 and 3.0. Such a range is typical of the warm dense regime and turns out to be accessible to experiments. In our average-atom framework, this ionization means that the occupation numbers of subshells 1s, 2s and 2p are respectively 2, 2 and 6, while the $n = 3$ electrons are in the continuum. This favorable situation avoids the use of unphysical non-integer bound occupation numbers in the subsequent photoionization cross-section calculation. The cases where the $n = 2$ core levels centered on different sites begin to overlap (for very high densities) or where discrete $n = 3$ levels begin to exist (in decompressed Al) are beyond the scope of our study. Moreover, our implementation of the MS photoionization theory that involves the preliminary construction of a muffin-tin potential is likely to be questionable when we leave the previously given range of density–temperature (section 4).

Before applying the previously described warm dense matter model to K-edge absorption profile calculations, we tested it against available x-ray diffraction data [39] and QMD simulation results [16, 17]. This concerns the static structure factor $\tilde{S}(q) = 1 + n_i\tilde{h}(q)$ of liquid Al near the melting point and also the radial distribution function (at a slightly lower density). Results are plotted in figures 1 and 2. We note a global agreement between x-ray values, QMD simulations and the present NPA-HNC calculations.

In figure 3, we display the calculated radial distribution function for slightly heated and solid density Al. The same quantity is plotted for slightly decompressed Al (figure 4) while various RDFs along the shock Hugoniot of Al are displayed in figure 5. In this last case, compression and temperature are connected via the equation of state [40]. These connected values are reported in figure 5.

3.4. Muffin-tin potential from selected ionic configurations and NPA charge densities

The absorber and the neighboring atoms define a cluster for which we have to calculate the initial state and the whole set

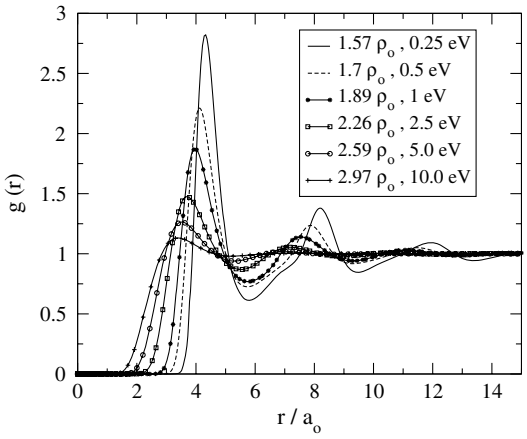

Figure 5. The ion–ion RDF of Al along the shock Hugoniot. The corresponding couples (ρ, T) are indicated in the box.

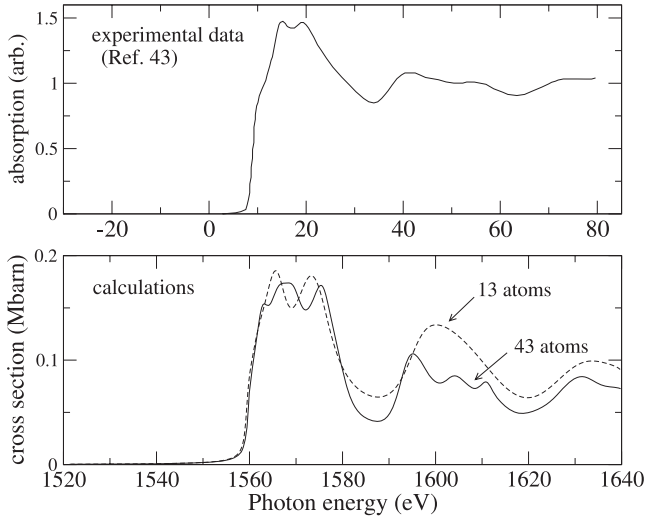

Figure 6. Solid-state (cold) Al K-edge spectrum. Top—experiment [43], bottom—calculation for two sizes of fcc cluster. Calculated spectra do not take into account any experimental broadening and ignore time-dependent screening effects in the response of the core hole.

of final state wavefunctions (depending on the photoelectron energy). A preliminary point in the application of the MST is the building of the potential. As in standard calculations of XANES spectra for solid-state materials we used the 'muffin-tin potential' approximation. In this approximation, the potential is spherically averaged in the atomic regions and volume averaged in the interatomic region. Standard prescriptions for the construction of a muffin-tin potential go back to Mattheiss's work [41] concerning energy band calculations in metals, and a clear explanation of its application to XAFS spectra can be found in [42]. The essence of this approximation is in the superposition of preliminary calculated *free neutral atom* electron densities placed at some definite spatial positions. In this work we go slightly beyond this prescription by using two kinds of actual NPA (and not free atom) electron densities: one specific density for the neighboring Al^{3+} ions (embedded in a jellium vacancy) and one specific density for the absorbing Al^{4+} ion (with a 1s core hole). This NPA-based muffin-tin construction of the potential is consistent with the dense matter model discussed in the previous section and prevents us from using *free atom* electron densities calculated with heuristic bound electron configurations. It is worth noting that this is a fully 'relaxed' and 'screened' construction of the potential seen by the photoelectron. To check the validity of this construction for a fixed geometry, we calculated XANES K-edge spectra of solid face-centered-cubic (fcc) aluminum for two different size of clusters. The results are plotted in figure 6 (bottom) and compared with available experimental data obtained on a synchrotron [43] (top). The $N = 43$ result compares quite well with the experimental result, thus indicating the correctness of the NPA-based approach and of our full-MS implementation. An important detail of these calculations is the exchange–correlation potential used in the calculation of the photoelectron wavefunction. To be consistent with the structural calculations (section 3.2), we used here the simple Kohn–Sham functional. More sophisticated functionals that depend on the kinetic energy of the photoelectron exist. In this case, the implementation of the exchange–correlation potential within the muffin-tin approximation deserves special attention [44].

We shall now discuss the determination of the spatial atomic positions from the above dense matter model applied to (disordered) warm dense aluminum. Unlike combined approaches based on MST and molecular dynamics simulations (and applied to solid amorphous media) [45, 46], the full DFT approach previously described gives only mean quantities like the $g(r)$ function. So, one must resort to a procedure for determining the atomic positions in a given cluster. In other words, one has to find the spatial configurations that 'sample' the $g(r)$ function. The way we set up this arrangement for a cluster of N atoms is now explained. We first consider the whole box of volume L^3 such that $L^3 = Na^3$, where a is the volume of the elementary cell ($\rho a^3 = 1$). In this box, one can select random configurations $\{(x_i, y_i, z_i), i = 1, N\}$, and for each N-atom configuration the $N(N-1)/2$ interatomic distances R_{ij} can be obtained. Noting that $4\pi r^2 g_{\rm trial}(r)\,{\rm d}r$ is the probability of finding an atom between r and $r + {\rm d}r$, an histogram can be built from the set $\{R_{ij}\}$, and the radial distribution function $g_{\rm trial}(r)$ be extracted. This $g_{\rm trial}(r)$ can now be compared with the calculated $g(r)$. Here we have chosen to retain N-atom configurations such that

$$\chi^2 = \sum_{i<j} |g_{\rm trial}(R_{ij}) - g(R_{ij})|^2 \qquad (19)$$

is as small as possible. From a practical point of view, the sampling of $g(r)$ over a reasonable distance (a few oscillations) with clusters having a moderate number of atoms may lead to duplicating a cluster in the three spatial directions according to the minimum image principle. Moreover, the random search for the best N-atom configurations, i.e. minimizing the χ^2, can be improved by applying a standard minimization procedure acting on the $3N$ coordinates of the cluster.

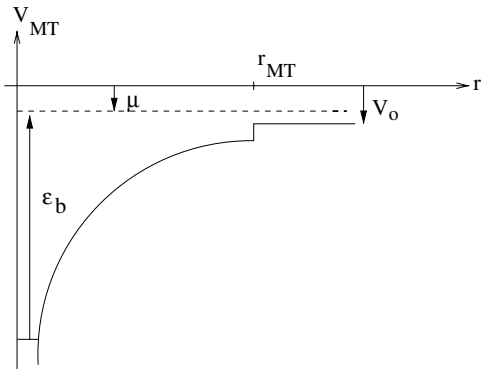

Figure 7. Muffin-tin potential around the photoionizing atom. V_o is the interstitial potential, μ is the chemical potential and ϵ_b is the bound energy of an inner-shell electron. r_{MT} is the muffin-tin radius. At $r = r_{MT}$, there is a small discontinuity inherent to the MT construction of the potential.

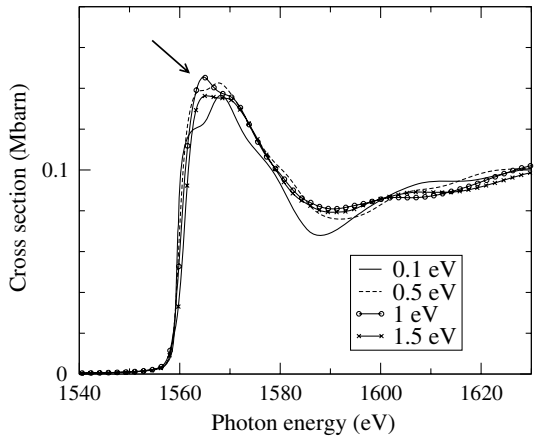

Figure 8. Temperature dependence of the Al XANES K-edge spectrum at solid density. The numbers in the inset are the different temperatures in eV.

An important quantity that remains to be defined is the muffin-tin radius r_{MT}, i.e. the radius attributed to each atom prior to constructing the muffin-tin potential. This is a free parameter whose determination is somewhat arbitrary. It is admitted (at least for solid-state calculations) that a small overlap of the spheres allows one to reduce the size of the interstitial region and also to minimize the discontinuities between the potential of the atomic spheres and the interstitial potential V_o. In the same vein and, after a few trials, we chose to attribute to r_{MT} half the value of an interatomic distance r corresponding to the maximum of the $g(r)$ function. However, in compressed matter, it seems necessary to consider interatomic distances rather located in the 'foot' of the $g(r)$ function ($0.15 g_{max}$). For all of the cases studied below in this paper, these values warrant the obvious requirement on the chemical potential $\mu > V_o$ in the construction of the muffin-tin potential (see figure 7). This point is clarified in the following paragraph.

3.5. Position of the threshold

In this paragraph, we address the difficult problem of the exact position of the edge and not only its shape. We mean here the localization in energy at the onset of absorption for zero temperature. Such a problem is better visualized by plotting the muffin-tin potential around the photo-absorbing atom (figure 7). At $T = 0$, the absolute value of ϵ_b is the 'true' bound energy (relative to the Fermi level) of a 1s electron if we look at a K edge. At this point, we must be aware that the approach followed in the previous sections was in fact based on a one-electron Kohn–Sham picture. Of course, the question of the value of ϵ_b cannot be addressed correctly with such a picture. This is truly a complicated multiparticle problem. In a DFT framework, only differences of 'ground energies' can be involved between an initial state i and a final state f. For the cases we consider in this paper, the initial state is the configuration $1s^2 2s^2 2p^6 +$ a thermally averaged set of unbound configurations for the remaining electrons. In other words, we have a $1s^2 2s^2 2p^6$ Al^{3+} ion imbedded into a jellium having a mean electron density $\bar{n} = Z^* n_i$ with $Z^* = 3$. Conversely, the final state has a 1s core hole, i.e. corresponds to a $1s2s^2 2p^6$ Al^{4+} ion imbedded into a jellium with $Z^* = 4$. The simplest way we address the calculation of ϵ_b at any T (in the range where $Z^* = 3$) is the Slater's transition state method [47]. In this context, we identify ϵ_b (see figure 7) with the value $\epsilon_b = \mu^{1/2} - \epsilon_{1s}^{1/2} + \Delta_o$, where $\epsilon_{1s}^{1/2}$ (< 0) is the orbital energy of a 1s electron in the fictitious $1s^{1.5} 2s^2 2p^6$ ion imbedded into a jellium of charge $Z^* = 3.5$ ($\mu^{1/2}$ is the corresponding chemical potential). Δ_o is a corrective shift to be adjusted. For Al, the value $\Delta_o = 1.2$ eV has been chosen in order to reproduce the commonly accepted value of the K-edge position at $T = 0$. We kept this value constant throughout the present calculations. Finally, in the present muffin-tin picture (see figure 7), we define the chemical potential as

$$\mu = \mu_{eg}(n_o, T) + V_o \tag{20}$$

where n_o and V_o are the mean interstitial electron density and the mean interstitial potential, respectively. μ_{eg} is the corresponding chemical potential for the uniform electron gas. Equation (20) is the straightforward finite-temperature generalization of the chemical potential proposed by Mustre de Leon *et al* [48].

4. Calculated warm dense K edges and discussion

Following the procedure described in the previous paragraphs, XANES spectra of the K edge in warm dense aluminum have been calculated. For each case characterized by ρ, T and its specific RDF function, 20 clusters of N atoms have been built. The disordered geometrical structure (and its associated muffin-tin potential) of each cluster has been determined following the procedure of section 3. We chose $N = 13$ as a significant value in a disordered medium (note that the whole $g(r)$ is sampled by using the minimum image principle). For each cluster, a XANES spectrum has been calculated using the full-MS formalism (section 2). Then, for each case, an average over 20 spectra has been performed. All the results are displayed in figures 8–10.

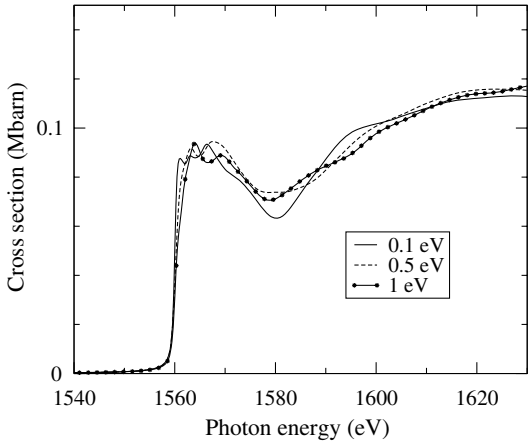

Figure 9. Temperature dependence of the Al XANES K-edge spectrum at $\rho_o/2$. The numbers in the inset are the different temperatures in eV.

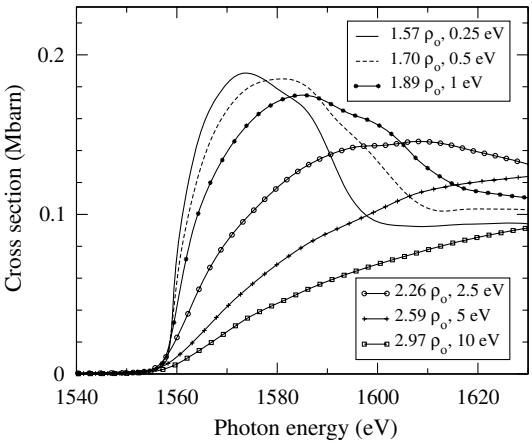

Figure 10. The Al XANES K-edge spectrum along the shock Hugoniot. The numbers in the insets are the different couples of density (in the unit of the solid density ρ_o)–temperature (in eV).

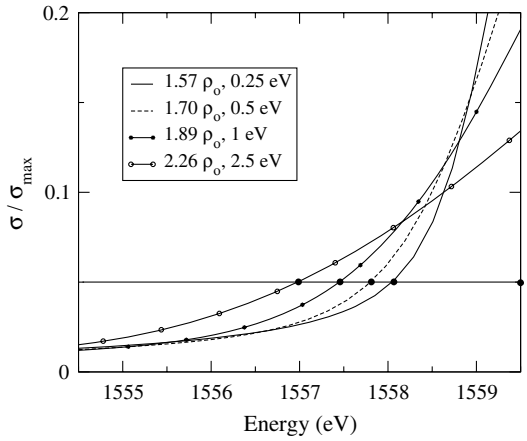

Figure 11. Zoom of the normalized edge profile (σ/σ_{max}) at the onset of absorption. The horizontal line is the preassigned value $\sigma/\sigma_{max} = 0.05$ (supposed to be observable). Intersection of the spectrum with the line indicates the shift relative to the position of the normal (solid) position of the Al K edge (located on the right axis). The numbers in the inset are the different couples of density (in the unit of the solid density ρ_o)–temperature (in eV).

Figure 8 shows the temperature dependence of the K-edge spectrum at solid density ρ_0. Figure 9 exhibits this dependence for $\rho_0/2$ while figure 10 shows the variation of the K edge along the shock Hugoniot. A first general comment is that the position of this edge (at the onset of absorption) has a complex behavior because it depends both on the energy of the core electron with respect to the chemical potential and on the progressive spreading of the Fermi function as the temperature increases. Any comparison with possible experiments in the warm dense regime is thus not easy, for it involves a criterion for the determination of the threshold. The inflexion point on the left side of the spectrum is one of the possible criteria but, at high temperature, it is very different from the onset of absorption and this reflects the lack of a true edge. Independently, the second structure in the K edge (observed around 1590 eV at zero temperature, figure 6) is not seen in the melted, disordered Al. More interesting is the existence and the position of the main peak observed is these spectra. In figure 8 this peak (indicated by an arrow) broadens while T increases. In the decompressed material (figure 9) one observes a reduction of this peak. In this case, for temperatures greater than about 1 eV, the obtained value of μ relative to V_o makes the muffin-tin approximation highly questionable (and then no results are shown), but this peak is likely to disappear. This progressive disappearance beyond a few eV is also observed in the compressed material (figure 10). Also, along the shock Hugoniot, it is worth noting a clear shifting and broadening of the main peak with compression. At the same time, and despite the non-existence of a true edge in the high-temperature regime, it is possible to study the observable position of the onset of absorption. The observable shift is defined as that value of the photon energy where the absorption coefficient (or the cross-section) scaled by the maximum value in the edge profile, $\sigma(E)/\sigma_{max}$, is a preassigned value (0.05 for instance) [13]. In the compressed aluminum, examples of such (red-) shifts are displayed in figure 11.

5. Conclusion

We have calculated the K-edge absorption of aluminum in the warm dense regime. Our approach is essentially a three-step procedure. The first step consists in using a DFT model of dense matter that has proven to be fruitful at least for the description of simple liquid metals and simple dense plasmas as well. Such an approach gives only thermodynamic averaged structural quantities like the radial distribution function $g(r)$. So the second step consists simply in extracting spatial atomic configurations (for a finite number of atoms defining a cluster) that are compatible with the previously calculated $g(r)$ function. In the third step, a muffin-tin potential is built and a full multiple-scattering calculation is applied in order to construct the XANES portion of the photoabsorption spectrum. Such a spectrum is averaged over a significant number of atomic configurations (or clusters). The warm dense regime we chose (ρ varies between $\rho_o/2$ and $3\rho_o$ while T is

between 0.1 and 10 eV) is likely to be studied in laboratory experiments, and these calculations indicate the modifications of the K-edge XANES spectra that can be expected. The dense matter model we used contains many ingredients and there is room for improvements. Furthermore, the K-edge calculation has identified weaknesses such as the muffin-tin approximation and the use of an approximate form of the chemical potential based on the free electron gas model. This is supposedly correct for simple metals and noble metals so one may expect the same in the warm dense regime. A possible improvement would be a more consistent determination of the chemical potential [49]. But still, in the decompressed matter at temperatures greater than about 1 eV, the MT approach is probably highly questionable. However, our approach as a whole has the advantages of being fast (compared with QMD calculations) and of giving a clear physical insight into the various involved phenomena. Future confrontations with experiments (and QMD calculations) should help in improving this kind of approach and this will improve our knowledge of the warm dense state of matter.

Acknowledgment

The author thanks J C Gauthier for useful comments on the manuscript.

References

[1] Ng A, Parfeniuk D, Celliers P, DaSilva L, More R M and Lee Y T 1986 *Phys. Rev. Lett.* **57** 1595
[2] Milchberg H M, Freeman R R, Davey S C and More R M 1988 *Phys. Rev. Lett.* **61** 2364
[3] Polischuk A Ya, Hloposin V S and Fortov V E 1991 *Phys. Lett.* A **157** 406
[4] Ng A, Celliers P, Forsman A, More R M, Lee Y T, Perrot F, Dharma-wardana M W C and Rinker G A 1994 *Phys. Rev. Lett.* **72** 3351
[5] Renaudin P, Blancard C, Faussurier G and Noiret P 2002 *Phys. Rev. Lett.* **88** 215001
[6] Glenzer S H, Gregori G, Rogers F J, Froula D H, Pollaine S W, Wallace R S and Landen O L 2003 *Phys. Plasmas* **10** 2433
[7] Perrot F and Dharma-wardana M W C 1987 *Phys. Rev.* A **36** 238
[8] Desjarlais M P, Kress J D and Collins L A 2002 *Phys. Rev.* E **66** 025401(R)
[9] Dharma-wardana M W C 2006 *Phys. Rev.* E **73** 036401
[10] Faussurier G, Blancard C, Renaudin P and Silvestrelli P L 2006 *Phys. Rev.* B **73** 075106
[11] Godwal B K, Ng A, DaSilva L, Lee Y T and Liberman D A 1989 *Phys. Rev.* A **40** 4521
[12] Hall T A, Al-Kuzee J, Benuzzi A, Koenig M, Krishnan J, Grandjouan N, Batani D, Bossi S and Nicolella S 1998 *Europhys. Lett.* **41** 495
[13] Perrot F and Dharma-wardana M W C 1993 *Phys. Rev. Lett.* **71** 797
[14] Tzortzakis S, Audebert P, Renaudin P, Bastiani S, Geindre J-P, Chesnais C, Nagels V, Shepherd R, Gary S, Matsushima I, Peyrusse O and Gauthier J-C 2006 *J. Quant. Spectrosc. Radiat. Transfer* **99** 614
[15] Kwon I, Collins L, Kress J and Troullier N 1996 *Phys. Rev.* E **54** 2844
[16] Silvestrelli P L 1999 *Phys. Rev.* B **60** 16382
[17] Alemany M M G, Gallego L J and Gonzalez D J 2004 *Phys. Rev.* B **70** 134206
[18] Mazevet S, Desjarlais M P, Collins L A, Kress J D and Magee N H 2005 *Phys. Rev.* E **71** 016409
[19] Clerouin J, Laudernet Y, Recoules V and Mazevet S 2005 *Phys. Rev.* B **72** 155122
[20] Natoli C R, Misemer D K, Doniach S and Kutzler F W 1980 *Phys. Rev.* A **22** 1104
[21] Natoli C R, Benfatto M and Doniach S 1986 *Phys. Rev.* A **34** 4682
[22] Sainctavit Ph, Cabaret D and Briois V 2006 Multiple scattering theory applied to x-ray absorption near edge structure *Neutron and X-ray Spectroscopy* ed F Hippert *et al* (Netherlands: Springer)
[23] Durham P J, Pendry J B and Hodges C H 1982 *Comput. Phys. Commun.* **25** 193
[24] Vvedensky D D, Saldin D K and Pendry J B 1986 *Comput. Phys. Commun.* **40** 421
[25] Neddermeyer H 1973 *Phys. Lett.* A **44** 181
[26] Penn D R 1987 *Phys. Rev.* B **35** 482
[27] Privalov T, Gel'mukhanov F and Agren H 2001 *Phys. Rev.* B **64** 165115
[28] Ankudinov A L, Nesvizhskii A I and Rehr J J 2003 *Phys. Rev.* B **67** 115120
[29] Perrot F 1990 *Phys. Rev.* A **42** 4871
[30] Ziman J M 1964 *Adv. Phys.* **13** 89
[31] Chabrier G and Perrot F 1991 *Phys. Rev.* A **43** 2879
[32] Rosenfeld Y and Ashcroft N W 1979 *Phys. Rev.* A **20** 1208
[33] Verlet L and Weiss J J 1972 *Phys. Rev.* A **5** 939
[34] Malijevsky A and Labik S 1987 *Mol. Phys.* **60** 663
[35] Lado F, Foiles S M and Ashcroft N W 1983 *Phys. Rev.* A **28** 2374
[36] Moroni S, Ceperley D M and Senatore G 1995 *Phys. Rev. Lett.* **75** 689
[37] Taylor R 1978 *J. Phys. F: Met. Phys.* **8** 1699
[38] Manninen M, Jena P, Nieminen R M and Lee J K 1981 *Phys. Rev.* B **24** 7057
[39] *IAMP Database of SCM-LIQ* Tohoku University http://www.iamp.tohoku.ac.jp/database/scm
[40] Kerley G I 1991 *Report Sandia No 88-2291 UC-405* unpublished
[41] Mattheiss L F 1964 *Phys. Rev.* A **134** 970
[42] Natoli C R, Benfatto M, Della Longa S and Hatada K 2003 *J. Synchrotron Radiat.* **10** 26
[43] Wong J, George G N, Pickering I J, Rek Z U, Rowen M, Tanaka T, Via G H, DeVries B, Vaughan D E W and Brown G E 1994 *Solid State Commun.* **92** 559
[44] Shneerson V L, Tysoe W T and Saldin D K 1995 *Phys. Rev.* B **51** 13015
[45] Cabaret D, Le Grand M, Ramos A, Flank A-M, Rossano S, Galoisy L, Calas G and Ghaleb D 2001 *J. Non-Cryst. Solids* **289** 1
[46] Levelut C, Cabaret D, Benoit M, Jund P and Flank A-M 2001 *J. Non-Cryst. Solids* **293** 100
[47] Slater J C 1974 *Quantum Theory of Molecules and Solids Spectral Lines* vol IV (New York: McGraw-Hill)
[48] Mustre de Leon J, Rehr J J, Zabinsky S I and Albers R C 1991 *Phys. Rev.* B **44** 4146
[49] Ankudinov A L, Ravel B, Rehr J J and Conradson S D 1998 *Phys. Rev.* B **58** 7565